From Kondo semimetal to spin-glass behavior in doped CeNi1-[delta]Sn1+[delta]-xSbx system

Andrzej Slebarski, Jozef Spalek

From Kondo semimetal to spin-glass behavior in doped CeNi1-[delta]Sn1+[delta]-xSbx system

Journal:	*Philosophical Magazine & Philosophical Magazine Letters*
Manuscript ID:	TPHM-08-Sep-0323.R1
Journal Selection:	Philosophical Magazine
Date Submitted by the Author:	03-Nov-2008
Complete List of Authors:	Slebarski, Andrzej; University of Silesia, Institute of Physics Spalek, Jozef; Jagiellonian University, M.Smoluchowski Institute of Physics
Keywords:	correlated systems, Kondo effect, quantum critical phenomena
Keywords (user supplied):	correlated systems, Kondo effect, quantum critical phenomena
Note: The following files were submitted by the author for peer review, but cannot be converted to PDF. You must view these files (e.g. movies) online.	
Phi-Mag_Slebarski-Spalek-last_2.tex	

From Kondo semimetal to spin-glass behavior in doped CeNi1-[delta]Sn1+[delta]-xSbx system

Journal:	*Philosophical Magazine & Philosophical Magazine Letters*
Manuscript ID:	TPHM-08-Sep-0323.R1
Journal Selection:	Philosophical Magazine
Date Submitted by the Author:	03-Nov-2008
Complete List of Authors:	Slebarski, Andrzej; University of Silesia, Institute of Physics Spalek, Jozef; Jagiellonian University, M.Smoluchowski Institute of Physics
Keywords:	correlated systems, Kondo effect, quantum critical phenomena
Keywords (user supplied):	correlated systems, Kondo effect, quantum critical phenomena
Note: The following files were submitted by the author for peer review, but cannot be converted to PDF. You must view these files (e.g. movies) online.	
Phi-Mag_Slebarski-Spalek-last_2.tex	

From Kondo semimetal to spin-glass behavior in doped $CeNi_{1-\delta}Sn_{1+\delta-x}Sb_x$ system

Andrzej Ślebarski[1] and Jozef Spałek[2]

[1] Institute of Physics, University of Silesia, 40-007 Katowice, Poland
E-mail: andrzej.slebarski@us.edu.pl
[2] Marian Smoluchowski Institute of Physics, Jagiellonian University, Reymonta 4, 30-059 Kraków, Poland
E-mail: ufspalek@if.uj.edu.pl

Abstract.

We investigate the properties of the off-stoichiometric $CeNi_{1-\delta}Sn_{1+\delta-x}Sb_x$ systems with $\delta \approx 0.06$ and $0 < x \leq 0.22$. Such a semimetallic $CeNi_{1-\delta}Sn_{1+\delta-x}Sb_x$ system is shown to transform into a Kondo semiconductor upon the substitution of about 2% of Sb for Sn. The effects of Sb doping on the low-temperature properties of CeNiSn were studied by means of electrical resistivity, magnetic susceptibility and specific heat. We interpret the ground state properties of the series of $CeNi_{1-\delta}Sn_{1+\delta-x}Sb_x$ compounds as resulting from the carrier number change acting together with the hybridization between the $4f$ electrons and the conduction electrons. For the Kondo semiconductor state we observe the scaling law $\chi\rho = const$ of the susceptibility χ and the resistivity ρ, which is regarded the basic feature for this class of materials, as was reported earlier. The magnetic properties of the system gradually evolve from the Kondo semimetallic state to the spin-glass behavior when the Sb doping increases.

PACS numbers: 71.27.+a, 72.15.Qm, 71.30+h

1. Introduction

Heavy fermion materials containing Ce display several distinct ground states [1], which depend crucially on a delicate balance between the competing Ruderman-Kittel Kasuya-Yosida (RKKY) and Kondo interactions [2]. Among possible ground states there is a low-carrier Kondo-lattice system CeNiSn, which has a small pseudogap in the electronic density of states at the Fermi level. Very recently, we have reported [3] that for $CeRhSb_{1-x}Sn_x$ system the formation of the Kondo-insulator gap is caused by the formation of a collective spin-singlet state, which is directly evidenced by the magnetic susceptibility behavior $\chi(T) \to 0$, and the activated behavior of the resistivity $\rho(T)$, both with $T \to 0$. Furthermore, the universal scaling law $\rho(T)\chi(T) = const$ is obeyed in the low-temperature region. From the experimental point of view, the above three features namely, the activated behavior of $\rho(T)$, the reduction of $\chi(T)$, and $\rho(T)\chi(T) = const$, define [3] the Kondo semiconductor/insulator as $T \to 0$. CeRhSb is a good example of such a cerium-containing Kondo insulator with a very narrow energy gap of the order of 1 meV in the electronic density of states (DOS) [4, 5]. CeNiSn, however, does not fit into this class of compounds [5, 6]. The first measurements showed an activated behavior in electrical resistivity $\rho(T)$ below ~ 6 K [6], but very pure samples of CeNiSn have a semimetallic and anisotropic conductivity [7], whereas the susceptibility increases when $T \to 0$.

Subsequent improvements in sample quality show, as presented in detail here that the $CeNi_{1-\delta}Sn_{1+\delta-x}Sb_x$ system can be described as a Kondo semimetal or a hybridization-gap semiconductor depending on value of δ. A systematic study has also shown that the gap formation in CeNiSn is very sensitive to the magnitude of the hybridization V between the f-electron and conduction-electron (c) states. This can be visualized by, e.g., partial substitution of Cu, Pd or Pt for Ni (Refs [8, 9, 10]), which strongly suppresses the pseudogap and even leads to a long-range magnetic order. A cerium valency close to 3+ [11] is likely to explain the nearness to magnetism of CeNiSn and is observed not only in many doped samples, but also in undoped CeNiSn. There is also evidence for a magnetic phase transition below 6 K in the off-stoichiometric samples $CeNi_{1\pm\delta}Sn_{\mp}\delta$; $\delta \approx 0.05$ [12]. In particular, there is an interesting report that CeNiSn undergoes a transition from a normal semimetallic state to a magnetically ordered one under pressure [13]. Moreover, it has been also reported that, since the critical pressure for this transition is about 0.1 GPa, CeNiSn can be regarded as a system on the brink of a magnetic instability or *quantum critical point*.

To investigate in detail the appearance of magnetism in the doped CeNiSn system we study the series $CeNi_{1-\delta}Sn_{1+\delta-x}Sb_x$ and analyse its ground-state properties upon the substitution of Sb or the slight off-stoichiometry. In the course of the work we have discovered that a small substitution of Sb ($\sim 2\%$) for Sn in a off-stoichiometric $CeNi_{0.94}Sn_{1.06}$ stabilizes the Kondo-insulating state with the gap of magnitude $\Delta \sim 4$ K. In this manner we clarify the apparent disagreement between various authors concerning the Kondo-insulating or semimetallic nature of CeNiSn. This allows us also to detect the

collective-Kondo-state formation as a function of the increasing number of carriers in the systems investigated. We also argue, that the stability of paramagnetic vs. magnetic ground states in the series $CeNi_{1-\delta}Sn_{1+\delta-x}Sb_x$ is strongly dependent on the hybridization magnitude V, which is either of intersite (see Ref. [11]) or intrasite nature. The gap associated with the collective-Kondo spin-singlet-state formation is reflected also by an intrinsic magnetic susceptibility $\chi(T)$ reduction when lowering the temperature. Finally, we observe the fundamental scaling law $\rho(T)\chi(T) = const$, characteristic of Kondo semiconductors, as determined by us earlier for $CeRhSb_{1-x}Sn_x$ [3]. Here, we have found additionally, that the magnetic properties of the system evolve from a nonmagnetic Kondo-semimetallic state to a spin-glass behavior when the concentration of Sb in the $CeNi_{1-\delta}Sn_{1+\delta-x}Sb_x$ system is larger than $\sim 10\%$. In brief, our results show a rich variety of phases of nonstoichiometric $CeNi_{1-\delta}Sn_{1+\delta-x}Sb_x$ with changing of either δ or x.

This work has an additional motivation. Namely, in our previous work [3] we doped the Kondo insulator CeRhSb with Sn and observed a spectacular transition from the insulating state to a nonmagnetic non-Fermi liquid state with decreasing number of carriers (i.e., for the concentration $x = 0.12$ of Sn). Now, by starting from a nonmagnetic off-stoichiometric Kondo insulator and increasing the number of carriers by the substitution of Sb for Sn the residual gap of the Kondo-type persists to the highest possible concentrations $x \sim 0.2$ of Sb, but the system exhibits the properties of a spin glass. These results mean that the evolution from the Kondo insulating state into a non-Fermi liquid state may encompass a formation of a nonstandard magnetic state. But even then the proposed by us earlier [3] the scaling law $\rho(T)\chi(T) = const$ is obeyed for all of the doped systems, in the T range depending on the doping x.

2. Experimental details

Pure CeNiSn and CeNiSb samples were first prepared by arc melting. The dilute $CeNi_{1-\delta}Sn_{1+\delta-x}Sb_x$ alloys were then prepared by diluting nominal compositions of the master compounds. To ensure homogeneity, each sample was turned over and remelted several times and then annealed at 800 ^{o}C for 2 weeks. The Sn-rich samples were carefully examined by x-ray diffraction analysis and found to be single phase (ϵ-TiNiSn type structure belonging to a space group $Pnma$) for the $x < 0.22$ concentration range. The lattice parameters of the components x are practically not x-dependent because of similar atomic radia of Sn and Sb atoms.

Stoichiometry and homogeneity were checked by the microprobe technique (scanning microscope JSM-5410) and the deviations from the nominal composition were small but substantial. The CeNiSn sample has the composition $CeNi_{0.94}Sn_{1.06}$, when normalized to the Ce content. The same happens for all the remaining Sb-doped samples. The off-stoichiometry $CeNi_{1-\delta}Sn_{1+\delta-x}Sb_x$ samples with $\delta \leq 0.06$ were, however, homogeneous, except very small islands of highly non-stoichiometric Ce-Ni-Sn-Sb components (compare to the results in Ref. [14]).

A standard four-terminal *ac* technique was used to measure the resistance of each

sample.

The magnetic susceptibility was measured in the $1.9 - 300$ K regime by use of a commercial *ac* Lake-Shore susceptometer. The amplitude of the excitation field was 1 mT at a fixed frequency of 10 kHz. dc magnetic measurements were carried out in the temperature range from 1.8 to 300 K in applied magnetic fields up to 1 T employing a Quantum Design superconducting quantum interference device (SQUID) magnetometer.

The XPS (x-ray photoelectron spectroscopy) spectra were obtained with monochromatized Al $K\alpha$ radiation at room temperature using a PHI 5700 ESCA spectrometer. The spectra were measured immediately after cleaving the sample in a vacuum of 10^{-10} Torr. The spectra were calibrated according to Ref. [15]. Binding energies were referenced to the Fermi level ($\epsilon_F = 0$).

Specific heat measurements have been performed in a fully adiabatic calorimeter between 2.7 K and 30 K.

3. Electronic band structure

It has been controversial whether CeNiSn has a V-shaped type of DOS (i.e., has a pseudogap) or is a semimetal with low carrier density. Different experiments: NMR [16], specific heat [17], or high-resolution photoemission spectroscopy [18] have shown the appearance of a residual DOS at the Fermi level (ϵ_F) $10 - 100$ times larger than the corresponding value coming from band structure calculations [19].

In Fig. 1 we compare XPS valence-band (VB) spectra of $CeNi_{1-\delta}Sn_{1+\delta-x}Sb_x$, with $x = 0$, 0.06, and 0.18 with those for CeRhSb. The spectra are normalized by this way, that the background intensities of each spectrum in the energy range $-2 \div 0$ eV are the same. The XPS valence bands of CeNiSn and $CeNiSn_{1-x}Sb_x$ alloys are very similar and the intensities at $E = 0$ (at ϵ_F), are the same within the experimental resolution, whereas the energy distribution for the bands in CeRhSb are quite different. The most important result is that the DOS at ϵ_F for CeNiSn is ~ 1.8 times larger than that of CeRhSb, which suggests a stronger metallicity of CeNiSn.

Fig. 2 shows the Ce 3d XPS spectra obtained for the series of compounds $CeNi_{1-\delta}Sn_{1+\delta-x}Sb_x$. The two final-state contributions f^1 and f^2 are clearly observed and exhibit the spin-orbit splitting 18.6 eV. The f^2 components in the Ce 3d XPS spectra are attributed within the Gunnarsson-Schönhammer theory to the f-conduction electron hybridization [20, 21]. The energy Δ_{fs} which describes the hybridization part of the Anderson impurity Hamiltonian [22], is defined as $\pi V^2 N(\epsilon_F)$, where $N(\epsilon_F)$ is the DOS at the Fermi energy, and V is the magnitude of the hybridization matrix element. The Δ_{fs} can be estimated from the integrated intensity ratio $r = I(f^2)/(I(f^1) + I(f^2))$, calculated as a function of Δ_{fs} in [21]. The separation of the overlapping peaks in the Ce 3*d* XPS spectra is determined using the Doniach-Šunjić approach [23]. The intensity ratio provides a rather crude estimate of $\Delta_{fs} \sim 0.15$ eV for CeNiSn and ~ 0.25 eV for the $CeNiSn_{1-x}Sb_x$ samples with $x = 0.06$ and $x = 0.09$, respectively, which means that the hybridization energy increases rapidly with the Sb doping.

In order to determine the ground-state f-level occupation, n_f, from the $3d$ XPS spectra we use Fig.4 of Ref. [21], where the dependence of the intensity ratio $r' = I(f^0)/(I(f^0) + I(f^1) + I(f^2))$ on the f occupation is shown for $\Delta_{fs} = 120$ meV. The relative f^0 intensities of magnitude $r' < 0.06$ for CeNiSn and $r' = 0$ for the remaining $CeNiSn_{1-x}Sb_x$ compounds correspond to $n_f \sim 0.94$ and 1, respectively, within the accuracy better than 15%. Parenthetically, the occupation $n_f = 1$ corresponds to the valency Ce^{3+} and in consequence, to the localized nature of $4f^1$ state. This in turn, will lead to a magnetic behavior of the corresponding systems, as discussed in detail in what follows.

The stability of paramagnetic vs. magnetic ground states in the Kondo-lattice limit [24] is strongly dependent on the on-site hybridization magnitude V and the number of valence electrons n_e. Previous alloying studies showed, that substituting either Sb for Sn in CeNiSn [25] or Sn for Sb in CeRhSb [26], leads to a formation of a weak ferromagnetic Kondo-lattice or to the non-Fermi liquid ground states, respectively. Doradziński and Spałek [24] (DS) discussed possible magnetic phases in the periodic Anderson model and obtained the phase diagram on the $V - n_e$ plane, which is in a qualitative agreement with the experimental results on the series of Ce-ternary intermetallics [27]. In DS diagram CeNiSn is located on the line $n_e \approx 2$ in the Kondo-insulator region, very close to the critical value of $V \approx 0.3$ eV, which separates the KI and antiferromagnetic Kondo-insulator (AKI) phases (see Fig. 3). The high-resolution photoemission study of CeNiSn [11] indicates a nonzero DOS at ϵ_F, suggesting a semimetallic ground state. The XPS experiment also provides an evidence that the electronic states located at ϵ_F have a mixed character composed of the Ce $4f$, Ce$5d$, Ni$3d$, and Snsp states. The semimetallic nature of CeNiSn means also that a sizeable part of the hybridization between $4f$ and the remaining valence electrons is of the intersite nature, and can vanish in some directions in the $\mathbf{k}$ space, which means that the Kondo insulating gap can open up. When the Sb doping is small, the intraatomic part of V dominates, as observed in the low-T resistivity data, which display the activated behavior. In effect, the intraatomic Kondo coupling can become stronger. Let us assume that a small doping of Sb ($x \leq 0.02$) does not change much DOS, whereas it significantly increases Δ_{fs}. Then, the compound $x = 0.02$ has a stable KI state in the DS diagram. However, from the $3d$ XPS spectra it follows that for $x > 0.02$, Δ_{fs} is ~ 1.3 times larger compared to that of CeNiSn, whereas the specific heat data display the $\gamma \sim N(\epsilon_F)$ value about $2 - 3$ times larger in relation to that of CeNiSn. In result, Sb doping locates the samples $x > 0.02$ on the AKI line of the DS diagram. Therefore, the magnetic ground state could be formed simultaneously with the Kondo-pseudogap appearance.

Next, we comment a possible critical behavior in CeNiSn under external pressure [13]. In the DS diagram CeNiSn is located in the $V - n_e$ plane near the critical point, which separates the nonmagnetic KI and AKI states. Since the critical pressure P_c is of ~ 0.1 GPa, as was shown in Ref. [13], the residual DOS at the Fermi level increases twice at $P > P_c$. In consequence, the hybridization energy $V = [\Delta_{fs}/(\pi N(\epsilon_F)]^{1/2}$ decreases crossing the critical point on the $V - n_e \approx 2$ plane. In this speculation, one has to

assume that the hybridization energy Δ_{fs} increases too. However, it has a weaker P-dependence [13]. Note, a quantum critical behavior at the Kondo insulator-non-Fermi liquid boundary was observed as a function of x in the system $CeRhSb_{1-x}Sn_x$ [3]. The critical concentration $x_c \approx 0.12$ separates the semiconducting KI from the metallic NFL phases. The reason for the quantum critical behavior in CeNiSn and $CeRhSb_{1-x}Sn_x$ system is, however, different; in CeNiSn the pressure leads to the quantum critical point, while in the case of $CeRhSb_{1-x}Sn_x$, doping (i.e., the increasing number carriers) leads to quantum criticality at x_c. However, in both situations a weak magnetic moment was detected in the vicinity of the QCP.

4. Electrical resistivity and magnetic properties.

4.1. Resistivity

In Fig. 4 we display the temperature dependence of the electrical resistivity $\rho(T)/\rho(300K)$ versus lnT for the $CeNi_{1-\delta}Sn_{1+\delta-x}Sb_x$ samples [28]. The curves for $x < 0.18$ exhibit a well defined activated behavior $\rho \sim exp(\Delta/T)$, with the activation energies Δ shown in the phase diagram shown later. The substitution of Sb for Sn, which increases nominally the number of carriers, produces an enhanced activated behavior with the conductivity gap $\Delta \cong 4.6 \pm 0.1$ K for x in the range $0.02 \div 0.06$, as compared to the value of the overall gap $\Delta \cong 1.7 \pm 0.1$ K for the pure $CeNi_{0.94}Sn_{1.06}$ compound. In the concentration range $0.1 \div 0.14$, $\Delta \cong 3.7$ K and for larger Sb doping, Δ value rapidly decreases. For the compositions $x = 0.2$ and $x = 0.22$, $\rho \sim -lnT$ in the range $\sim 7 \div 25$ K, suggesting the Kondo-lattice type of behavior.

The most important fact is that the Sb impurities stabilize the semiconducting-gap state in $CeNi_{1-\delta}Sn_\delta$. The formation of the coherent state in the Kondo lattice could be studied by introducing disorder into the system investigated. The extreme sensitivity of $\rho(T)$ to nonmagnetic impurities is well known from the low-carrier compound $CePd_3$ [29]. These impurities are known as the Kondo holes and are experimentally realized by subtracting a Ce ion in a stoichiometric Ce compound by La or Th atoms [30, 31]. Adding impurities to a Kondo lattice gradually destroys the coherence of the HF ground state. The addition of Sb, however, can not be simply interpreted as adding Kondo holes, but rather as adding carriers. In this case, the fractional number of electrons needed to produce the semiconducting state (the case of the sample $x \approx 0.2$) could complete filling of a band in CeNiSn semimetal.

4.2. Susceptibility

In Fig. 5 we present the temperature dependence of *ac* magnetic susceptibility $\chi = (\chi^{'2} + \chi^{''2})^{1/2}$. For $CeNi_{1-\delta}Sn_\delta$ $\chi(T)$ is increasing with decreasing temperature. In the $T < 30$ K temperature range, $\chi(T) = \chi_0 + yC/(T-\theta)$, with $\chi_0 = 5.7 \times 10^{-4}$ emu/mol, the effective Curie constant $yC = 1.8 \times 10^{-3}$ emu/Kmol, and $\theta = -0.7$ K. In view of the circumstance, that the Curie constant for Ce^{3+} ion is $C = 0.807$ emu/Kmol, the

susceptibility upturn is due to Ce^{3+} interstitial impurities of the concentration $y \cong 0.3\%$ [32]. On the contrary, the samples with $x > 0$ display a pronounced downturn even without the subtraction of the Ce^{3+} impurity contribution, which we attribute to the formation of the collective Kondo-singlet type of state (cf. Fig. 4). The increase of χ for $x > 0$ at $T < 2.5$ K is regarded again as due to the impurity contribution. The χ_{dc} susceptibility of the samples with $x \geq 0.12$ has a sharp maximum at T_f (see Fig. 6*d*). T_f is x-dependent (not shown) and increases with increasing x, revealing the magnetic ordering of the spin-glass-type at approximately 3 K. A very similar behavior is often observed, when CeNiSn is doped [33], or defected [12]. It seems possible, that atomic disorder creates a spin glass-type state for the systems $CeNi_{1-\delta}Sn_{1+\delta-x}Sb_x$ having a nonzero pseudogap. To confirm this hypothesis, we have studied the zero-field cooled (ZFC) and the field cooled (FC) dc magnetic susceptibilities for the magnetic field of 100 Oe, as well as the ac magnetic susceptibility for the field amplitude of 3 Oe vs. frequency. In Fig. 6*d* we present the ZFC and FC dc magnetic susceptibilities $\chi \equiv M/H$ measured for $CeNi_{1-\delta}Sn_{0.84+\delta}Sb_{0.16}$. The $\chi(T)$ data display hysteretic features typically related to the development of a spin glass-like (SG) state below a freezing temperature T_f. A similar behavior was observed for other $CeNi_{1-\delta}Sn_{1+\delta-x}Sb_x$ samples with $x > 0.12$. Fig. 6$a-c$ displays the frequency dependent maxima of the real component $\chi^{'}$ of χ for the sample $x = 0.16$ [panel (b)], that are characteristic of the SG state. This behavior is observed for samples with smaller than 12% amount of Sb [see, panel (a)]. The imaginary component $\chi^{''}$ of χ indicates the appearence of a weak anomaly only at T_f for the low frequency of 50 Hz, whereas, it is almost constant for higher frequencies. The low-frequency susceptibility curves looks like those of a short-range antiferromagnet with a weak frequency dependence of $\chi^{'}$ and no change in $\chi^{''}$. Such a behavior of $\chi^{''}$ was reported [34] for the $Y_{1-x}U_xPd_3$ system, in which there is an interplay between the spin-glass and the non-Fermi liquid behavior, and is ascribed to the atomic-disorder. $\chi^{'}$ of $CeNiSn_{0.98}Sb_{0.02}$ shows a sharp upturn with decreasing T, consistent with the presence of paramagnetic impurities with concentration less than 2%. The dotted line is a fit the of modified Curie-Weiss law specified in the Figure caption.

Finally, in Fig. 6*c*, we present magnetization M versus H data, which show a hysteresis loop below T_f for $CeNi_{1-\delta}Sn_{0.84+\delta}Sb_{0.16}$; this behavior is not observed for $CeNi_{1-\delta}Sn_{1+\delta-x}Sb_x$ samples with $x < 0.12$.

All of these measurements strongly support the interpretation that there exists a spin-glass state in the compounds $CeNi_{1-\delta}Sn_{1+\delta-x}Sb_x$ containing more than 12% of Sb. The dc magnetic susceptibilities (cf. Fig. 7), measured for the series $CeNi_{1-\delta}Sn_{1+\delta-x}Sb_x$ of alloys, do not follow the Curie-Weiss law in the whole temperature range between 2 and 300 K. As is shown in Fig. 6*a*, the χ-curve exhibits a upturn below $\sim$ 10 K for paramagnetic samples with $x < 0.12$ due to the presence of impurities. Fig. 7 presents the dc susceptibility with the impurity contamination (yC/T) subtracted. This χ reduction when T is lowered is at least as evident as in that coming from the ac measurements (cf. Fig. 5)

In Fig. 8 we plot the scaling of the inverse resistivity ρ^{-1} vs. χ. This type of

scaling is spectacular for low concentrations $x = 0.02$ and $x = 0.06$, as was the case for $CeRhSb_{1-x}Sn_x$ [3]. We regard this as one of the fundamental properties of the Kondo semiconducting system. This $\rho\chi = const$ behavior is absent for $CeNi_{1-\delta}Sn_{1+\delta}$. This behavior has been explained in an elementary manner in [3].

4.3. Specific heat and the phase diagram

A direct evidence for strong electronic correlations in the present $CeNi_{1-\delta}Sn_{1+\delta-x}Sb_x$ system is provided by the large magnitude of the electronic specific heat coefficient $\gamma_0 \equiv C(T \to 0)/T$, which reaches the value of ~ 175 mJ/molK^2 for $x = 0.04$, 0.16 and 0.18. In Fig. 9, we plot the specific-heat $\Delta C/T$ data versus T on a log-log scale, where $\Delta C = C(CeNiSn_{1-x}Sb_x) - C(LaNiSn)$. By subtracting the heat capacity of pure LaNiSn, we observe a power-law increase of $\Delta C/T$ in the temperature range $5-14$ K, i.e., above the spin-glass-paramagnetic phase transition. The quasi-singular part of the specific heat in this T-regime is parametrized by the power-law $\Delta C/T = cT^{-n}$ (dotted lines in the figure) with exponent $n \approx 1$ for the samples $x = 0.16$ and 0.18, often observed for the spin glasses. For the sample $x = 0.04$ the exponent is $n \approx 0.5$ and this indicates the magnetic correlations set in at low temperatures, while at ~ 6 K $\Delta C/T$ exhibits a pronounced maximum which is linked to pseudogap formation at the HF Fermi level in $CeNi_{1-\delta}Sn_{0.96+\delta}Sb_{0.04}$. Moreover, $\Delta C/T \sim T$ in the $T \approx 2$ K regime below the maximum, which is evidence for the opening of a narrow pseudogap in this Kondo system [16]. In Fig. 9 $\Delta C/T$ also shows a feature at ~ 6 K for the remaining samples $x = 0.16$ and 0.18, that can be linked to the opening of the pseudogap in those disordered alloys.

Fig. 10 shows the overall phase diagram for the Sn-rich system $CeNi_{1-\delta}Sn_{1+\delta-x}Sb_x$ studied in this paper.

5. Physical discussion.

Although we did not find out evidence for the quantum critical behavior to the Kondo insulating state [3] as a function of the increasing Sb substitution for Sn (i.e., with the carrier concentration increase), several interesting new features appear. The stabilization of the Kondo gap/pseudogap state in $CeNi_{1-\delta}Sn_{1+\delta}$ semimetal and the role of atomic disorder and of the increased carrier concentration on the ground state properties seem to be important. In other words, we believe that the disorder created by the off-stoichiometry creates a gap, but the additional increase of the carrier concentration (via Sb addition) creates the true Kondo semiconducting state.

From the susceptibility data we know that almost all Ce^{3+} moments in the Kondo-insulator are compensated, i.e., the effect is of collective nature. At high temperature $T >\sim 50$ K [3], i.e., higher than the coherence temperature, the itineracy of the f electrons is destroyed by the thermal disorder. The coherence temperature T_K is about 30 K for CeNiSn, using the relation $T_K = 0.68R/\gamma$ [35]. In effect, the system

evolves from metal with localized f electrons at high temperature, through the heavy-Fermion (HF) phase, to the Kondo semimetal or insulator phase as $T \to 0$. The scaling $\chi \sim \rho^{-1}$ is expected to be observed for $T < T_K$, however, the $\chi\rho = const$ behavior is visible here in the limited T-range above the temperature T_f. The formation of the collective Kondo-singlet state in the KI or KS regimes is determined by reduction of the magnetic susceptibility in low-T range and presence of scaling $\chi(T)\rho(T) = const$. The presence of the spin-glass phase at $T < T_f$ means that the $4f$ localized moments are not compensated completely, so the semiconducting behavior is not as clear cut, as it is found in CeRhSb. It is possible, that the disorder creates localized states in the pseudogap of CeNiSn. However, it does not change drastically the activated behavior for $x < 0.1$, so we attribute the persistence of the KI state with the increasing hybridization gap at ϵ_F for the low x as a result of increased binding energy caused by the carrier concentration increase, with the concomitant f-electron localization at the lowest temperatures. In result, for small concentration of Sb (i.e., for $x \sim 0.02$) one could expect a gradual evolution from the heavy fermion state into the Kondo semiconductor at $T < \Delta$.

6. Acknowledgments

The authors are grateful to Mrs. Alicja Hackemer for her assistance during the heat capacity measurements. This work was partly supported by the COST P-16 European Network *Emergent Behaviour in Correlated Matters* (ECOM) and the National Scientific Network *Materials with Strongly Correlated Electrons* (MSSE). One of us (J.S.) acknowledges the Grant No 1 P03B 001 29 from the Ministry of Science and Higher Education.

[1] P.S. Reiseborough, Phys. Rev. B **45**,13984 (1992).
[2] S. Doniach, Physica B and C **91**, 231 (1977).
[3] A. Ślebarski and J. Spałek, Phys. Rev. Lett. **95**, 046402 (2005); J. Spałek, A. Ślebarski, J. Goraus, L. Spałek, K. Tomala, A. Zarzycki, and A. Hackemer, Phys. Rev. B, **72**, 155112 (2005).
[4] S. K. Malik and D. T. Adroja, Phys. Rev. B **43**, 6277 (1991).
[5] T. Ekino, T. Takabatake, H. Tanaka, and H. Fujii, Phys. Rev. Lett. **75**, 4262 (1995).
[6] T. Takabatake, F. Teshima, H. Fujii, S. Nishigori, T. Suzuki, T. Fujita, Y. Yamaguchi, J. Sakurai, and D. Jaccard, Phys.Rev.B **41**, 9607 (1990).
[7] T. Takabatake, G. Nakamoto, T. Yoshino, H. Fujii, K. Izawa, S. Nishigori, H. Goshima, T. Suzuki, T. Fujita, K. Maezawa, T. Hiraoka, Y. Okayama, I. Oguro, A.A. Menovsky, K. Neumaier, A. Brückl, and K. Andres, Physica B **223-224**, 413 (1996).
[8] T. Takabatake, Y. Nakazawa, M. Ishikawa, T. Sakakibara, K. Koga, and I. Oguro, J. Magn. Magn. Mater. **77-76**, 87 (1988).
[9] S. Nishigori, H. Goshima, T. Suzuki, T. Fujita, G. Nakamoto, T. Takabatake, H. Fujii, and J. Sakurai, Physica B**186-188**, 406 (1993).
[10] T. Takabatake, F. Iga, T. Yoshino, Y. Echizen, K. Katoh, K. Kobayashi, M. Higa, N. Shimizu, Y. Bando, G. Nakamoto, H. Fujii, K. Izawa, T. Suzuki, T. Fujita, M. Sera, M. Hiroi, K. Maezawa, S. Mock, H. vLhneysen, A. Brckl, K. Neumaier, and K. Andres, J. Magn. Magn. Mater. **177-181**, 277 (1998).
[11] J.-S. Kang, C.G. Olson, Y. Inada, Y. Onuki, S.K. Kwon, and B.I. Min, Phys.Rev.B **58**, 4426 (1998).
[12] F.G. Aliev, R. Villar, S. Vieira, R.V. Scolozdra, and T. Takabatake, Physica B**199-200**, 433 (1994).
[13] K. Umeo, T. Igaue, H. Chyono, Y. Echizen, T. Takabatake, M. Kosaka, and Y. Uwatoko, Phys. Rev B **60**, R6957 (1999).
[14] G. Nakamoto, T. Takabatake, H. Fujii, A. Minami, K. Maezawa, I. Oguro, and A. Menovsky, J. Phys. Soc. Japan, **64**, 4834 (1995).
[15] Y. Baer, G. Busch, and P. Cohn, Rev. Sci. Instrum. **46**, 466 (1975).
[16] K. Nakamura, Y. Kitaoka, K. Asayama, T. Takabatake, G. NakamotoH. Tanaka, and H. Fujii, Phys. Rev. B **53**, 6385 (1996)
[17] K. Izawa, T. Suzuki, T. Fujita, T. Takabatake, G. Nakamoto, H. Fujii, and K. Maezawa, Phys. Rev. B **59**, 2599 (1999)
[18] H. Kumigashira, T. Sato, T. Yokoya, T. Takahashi, S. Yoshii, and M. Kasaya, Physica B **281-282**, 284 (2000).
[19] A. Ślebarski, A. Jezierski, A. Zygmunt, S. Mähl, M. Neumann, and G. Borstel, Phys. Rev. B **54**, 13551 (1996).
[20] O. Gunnarsson and K. Schönhammer, Phys. Rev. B **28**, 4315 (1983).
[21] J. C. Fuggle, F. U. Hillebrecht, Z. Zolnierek, R. Lässer, Ch. Freiburg, O. Gunnarsson, and K. Schönhammer, Phys. Rev. B, **27**, 7330 (1983).
[22] P. W. Anderson, Phys. Rev. **124**, 41 (1961).
[23] S. Doniach and M. Šunjić, J. Phys. C **3**, 286 (1970).
[24] J. Spałek and R. Doradziński, in *Magnetism and electronic correlations in local-moment systems: rare earth elements and compounds*, edited by M. Donath, P. A. Dowben, and W. Nolting (World Stientific, Singapure, New Jersey, London, Hong Kong, 1998), p. 387; R. Doradziński and J. Spałek, Phys. Rev. B **56**, R14239 (1997); R. Doradziński and J. Spałek, Phys. Rev. B **58**, 3293 (1998); for brief review see: J. Spałek and R. Doradziński, Acta Phys. Polon. A **96**, 677 (1999); *ibid.* **97**, 71 (2000).
[25] L. Menon and S. Malik, Phys. Rev. B **52**, 35 (1990).
[26] A. Ślebarski, M. B. Maple, E. J. Freeman, C. Sirvent, M. Radłowska, A. Jezierski, E. Granado, Q. Huang, and J. W. Lynn, Phil. Mag. B **82**, 943 (2002).
[27] A. Ślebarski, J. Alloys Comp. **432**, 15 (2006).
[28] The plateau in the monocrystalline CeNiSn samples in the temperature dependence of $\rho(T)$ has

been observed, see: T.E. Mason, G. Aeppli, A.P. Ramirez, K.N. Clausen, C. Broholm, N. Stücheli, E. Bucher, and T.T.M. Palstra, Phys. Rev. Lett. **69**,490 (1992).

[29] J.M. Lawrence, T. Graf, M.F. Hundley, D. Mandrus, J.D. Thompson, A. Lacerda, M.S. Torikachwili, J.L. Sarrao, and Z. Fisk, Phys. Rev. B **53**, 12559 (1996).

[30] M.F. Hundley, P.C. Confield, J.D. Thompson, and Z. Fisk, Phys. Rev. B **50**, 18142 (1994).

[31] P. Schlottmann, Phys. Rev. B **46**, 998 (1992).

[32] The heat capacity and thermal expansion results showed a kink at about 6 K and a feature at about 2K. These anomalies were described as extrinsic and as originating from the presence of $CeNi_2Sn_2$ and $Ce_3Ni_4Sn_3$ impurities; see: Ref. [14]; G. Nakamoto, T. Takabatake, Y. Bando, H. Fujii, K. Izawa, T. Suzuki, T. Fujita, A. Minami, I. Oguro, L.T. Tai, and A.A. Menovsky, Physica B **206-207**,840 (1995)

[33] B. Buschinger, M. Weiden, O. Trovarelli, P. Hellmann, C. Geibel, and F. Steglich, J. Phys.:Condens. Matter **10**, 2021 (1998).

[34] M.A. Lopez de la Torre, J. Rodriguez Fernandez, K.A. McEven, and M.B. Maple, Phys. Rev. B **74**, 014431 (2006).

[35] L.N. Oliveira and J.W. Wilkins, Phys. Rev. Lett. **47**, 1553 (1981).

Figure 1. The valence band XPS spectra as a function of binding energy for the characteristic components of the series $CeNi_{1-\delta}Sn_{1+\delta-x}Sb_x$, with $\delta \approx 0.06$ ($x = 0$, 0.03, and 0.09). The spectrum of CeRhSb Kondo semiconductor is presented for comparison. The energy $E = 0$ represents the Fermi level position. The peak is due to the $4d$ states due to Rh or $3d$ states due to Ni.

Figure 2. The $3d$ Ce core-electron XPS spectra for $CeNi_{1-\delta}Sn_{1+\delta-x}Sb_x$ ($x = 0$, 0.06, and 0.18). The peaks are split by the spin-orbit interaction $\Delta_{SO} = 18.6$ eV.

Figure 3. Magnetic mean-field phase diagram on the plane: number of electrons per atom-hybridization (details in Ref. [24]). FM, WFM and SFM denote ferromagnetic, weakly ferromagnetic or strongly ferromagnetic metallic phases, respectively. AFM 1 and 2 represent different antiferromagnetic metallic phases, and PKI or AKI are paramagnetic or antiferromagnetic Kondo insulators, respectively. The point represents the experimental data for the Kondo lattice CeNiSn, which is experimentally obtained from the $3d$ Ce XPS spectra. In the $V = 0$ limit all the states have same energy, as no magnetic interaction within f system and between the systems ($f - c$) appears.

Figure 4. $CeNi_{1-\delta}Sn_{1+\delta-x}Sb_x$: *a*) temperature dependence of the resistivity normalized to the resistivity at 300 K. The presence of plateau indicates the impurity-band contribution; *b*) $ln\rho$ vs. $1/T$ showing explicitly the activated character for same samples.

Figure 5. $CeNi_{1-\delta}Sn_{1+\delta-x}Sb_x$: *ac* magnetic susceptibility vs temperature, measured in the applied field of amplitude $H_a = 10$ Oe. Note the reduction of the susceptibility for $0 < x < 0.1$, speaking for the Kondo singlet formation at low T. The off-stoichiometric system with $x = 0$ has a markedly different T dependence due to magnetic impurities.

Figure 6. $CeNi_{1-\delta}Sn_{1+\delta-x}Sb_x$: ($a$): real $\chi^{'}$ and imaginary $\chi^{''}$ components of ac magnetic susceptibility for $x = 0.02$. The other parameters are: $\delta \approx 0.06$, $\nu = 500Hz$, $H_a = 3$ Oe. The fit in (a) to the expression $\chi = \chi_0 + yC/(T - \theta)$ gives the fitting parameters: $\chi_0 = 4.4 \times 10^{-3}$ emu/mol, $y = 0.02$, and $\theta = -1.7$ K. In panel (b): $\chi^{'}$ and $\chi^{''}$ for $CeNi_{1-\delta}Sn_{0.84+\delta}Sb_{0.16}$ versus temperature and frequency is carried out in the applied field of 10 Oe. The panel (c) shows the magnetization M vs. magnetic field for the sample $CeNi_{1-\delta}Sn_{0.84+\delta}Sb_{0.16}$. The hysteresis loop is observed for $T < T_f$. The panel (d) exhibits temperature dependence of the zero-field cooled (ZFC) and field cooled (FC) dc susceptibility for the sample $CeNi_{1-\delta}Sn_{0.84+\delta}Sb_{0.16}$ in the field of 100 Oe.

Figure 7. ZFC dc magnetic susceptibility vs. T in the field of 100 Oe. The magnetic contribution yC/T is subtracted from the data. For all the samples the value $y = 0.015$ was taken. Note the characteristic downturn of $\chi(T)$ as the Kondo insulating state is approached, as marked by the dashed line.

Figure 8. Linear scaling law between the inverse resistivity ρ and the susceptibility χ for the samples with nonvanishing Kondo gap. The values of χ and ρ for different x are shifted to zero values at the minimal positions. The scaling law $\rho\chi = const$ is obeyed in the temperature range $5 \div 35$ K for $CeNi_{1-\delta}Sn_{1+\delta-x}Sb_x$.

Figure 9. $CeNi_{1-\delta}Sn_{1+\delta-x}Sb_x$, $\delta \approx 0.06$; specific heat $\Delta C/T$ versus T for samples with $x = 0.04$, 0.016, and 0.018 in the log-log scale; $\Delta C = C(sample) - C(LaNiSn)$. For $5 < T < 14$ K, $\Delta C(T)/T \sim T^{-n}$, with $n = 0.96$, 0.82, and 0.57 for samples $x = 0.16$, 0.18, and 0.04, respectively. The slope of the linear portion is marked by a dashed line in each case, it changes slightly in a nonsystematic manner and the overall value of n is approximately equal to unity, and regarded as typical for the spin-glass state.

Figure 10. Schematic phase diagram for $CeNi_{1-\delta}Sn_{1+\delta-x}Sb_x$ systems with $\delta = 0.06$. The activation energy Δ is obtained from the fit of expression $\rho(T) = \rho_0 exp(\Delta/T)$ to the resistivity data in the Kondo insulating/semimetallic regime (KS). T_{SG} is the temperature at the maximum of the χ ac data in the spin-glass (SG) state.

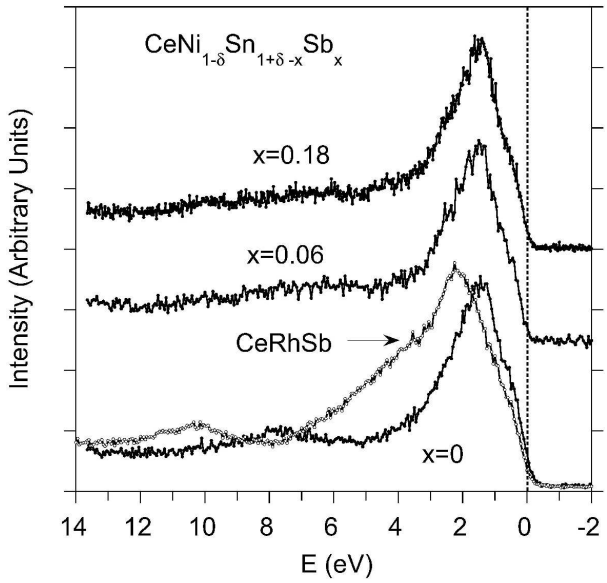

Figure 1
209x297mm (600 x 600 DPI)

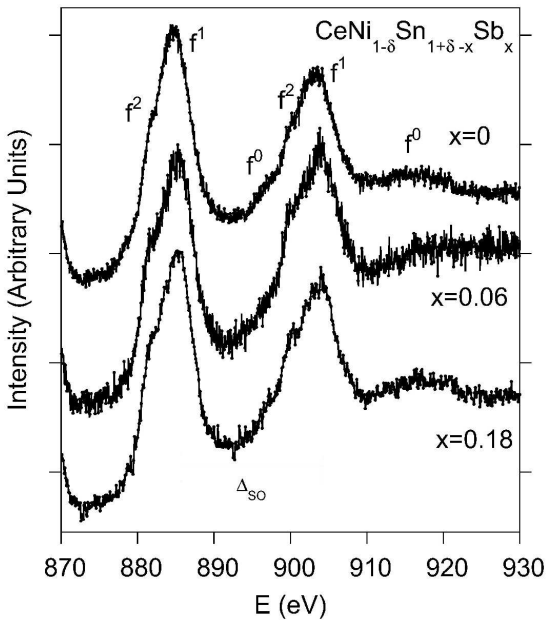

Figure 2
209x297mm (600 x 600 DPI)

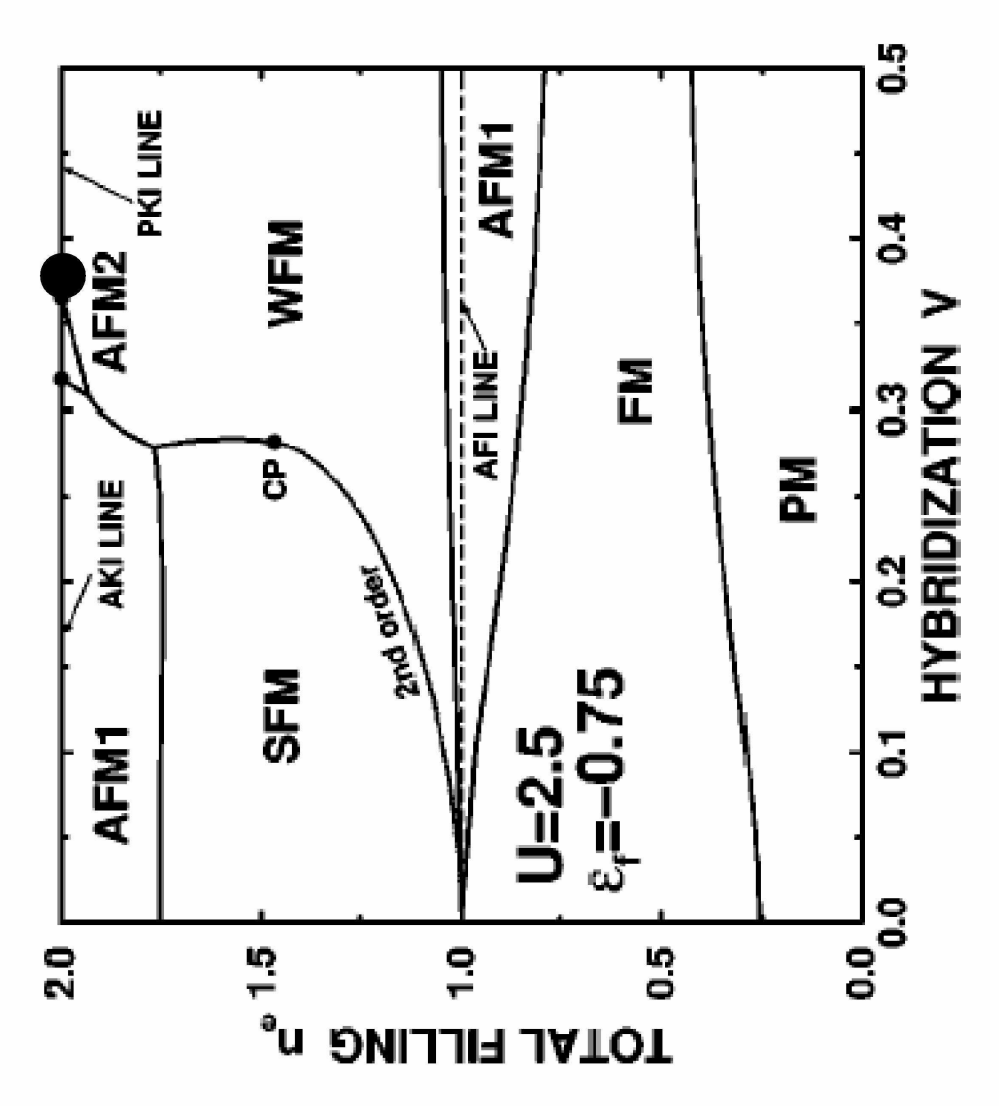

Figure 3
99x110mm (600 x 600 DPI)

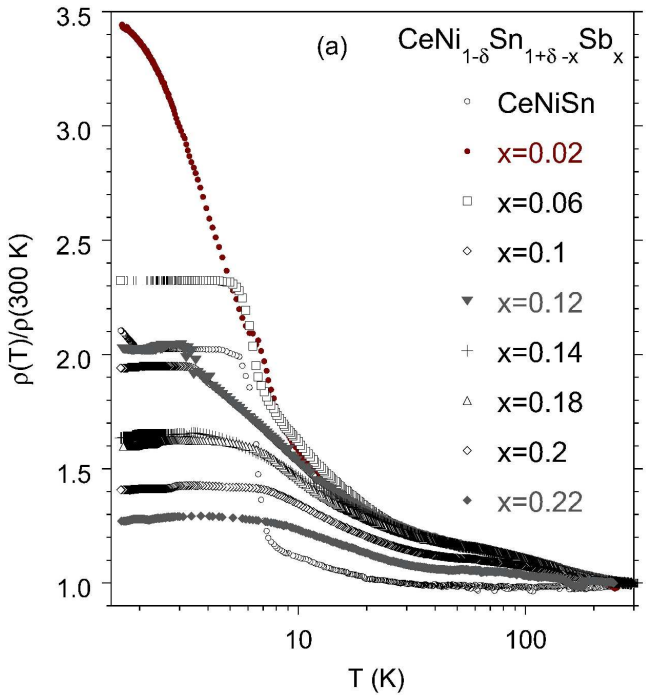

figure 4a
209x297mm (600 x 600 DPI)

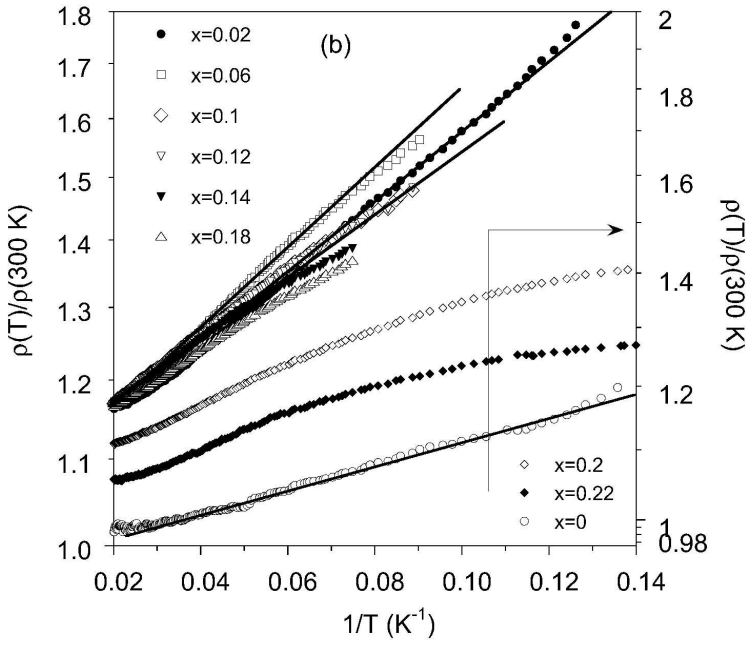

Figure 4b
209x297mm (600 x 600 DPI)

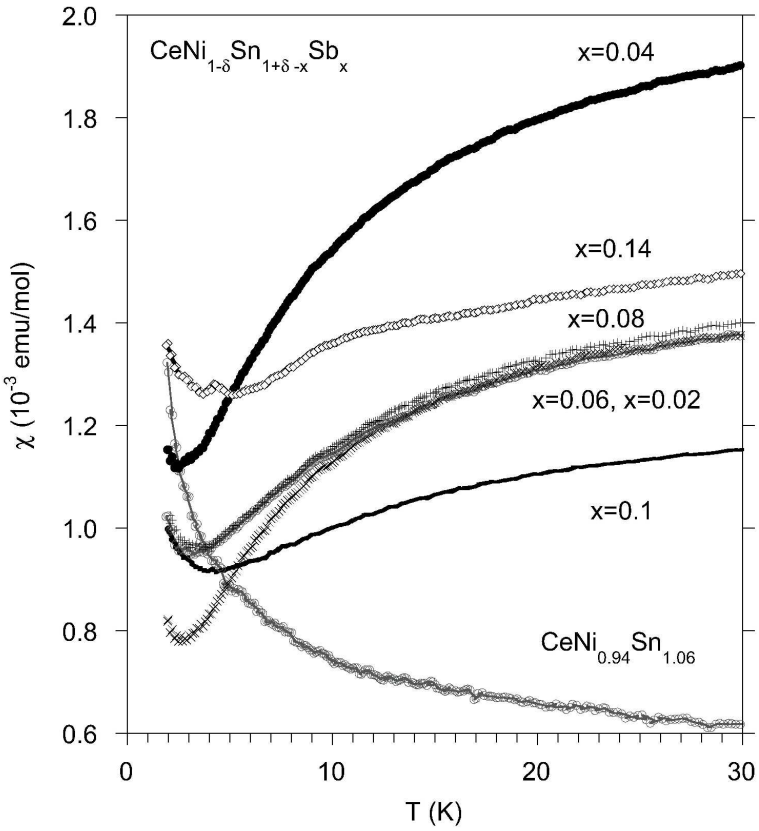

Figure 5
209x297mm (600 x 600 DPI)

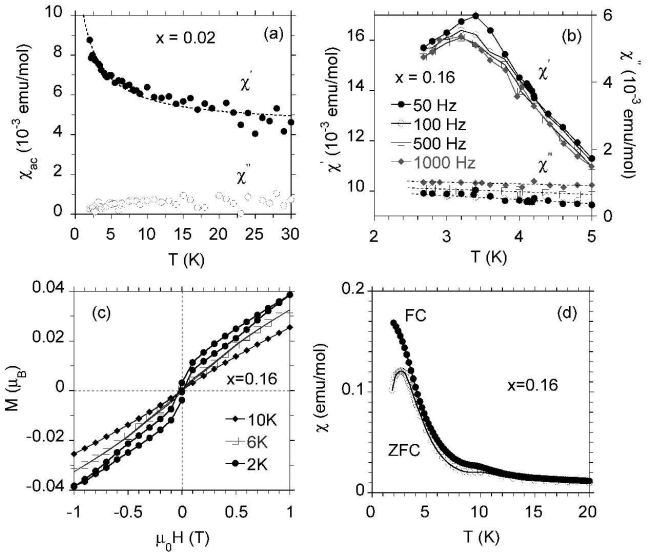

Figure 6
209x297mm (600 x 600 DPI)

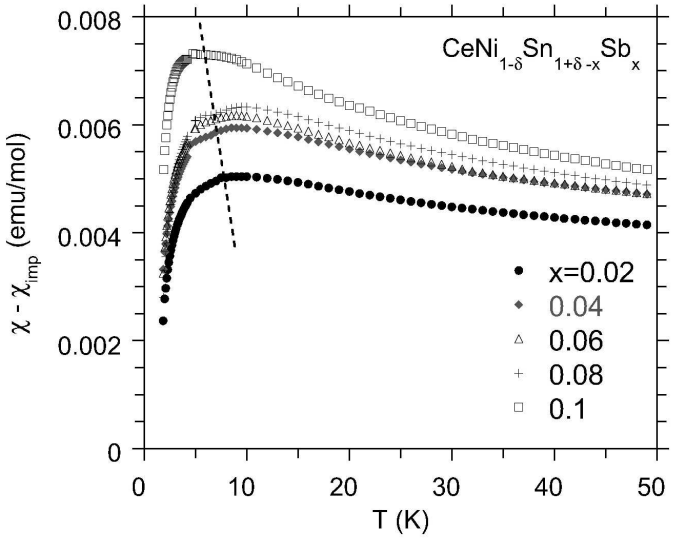

Figure 7
209x297mm (600 x 600 DPI)

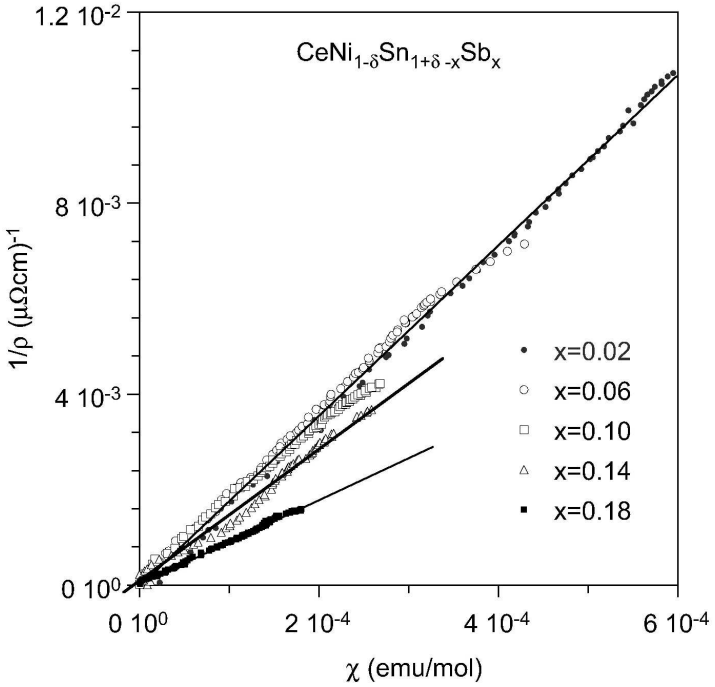

Figure 8
209x297mm (600 x 600 DPI)

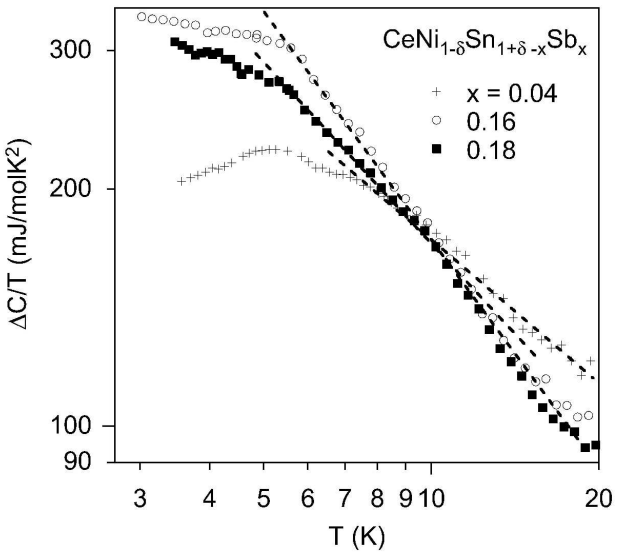

Figure 9
209x297mm (600 x 600 DPI)

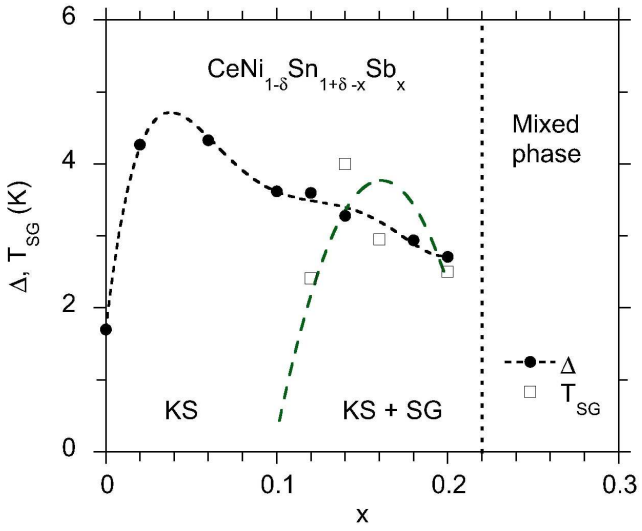

Figure 10
209x297mm (600 x 600 DPI)

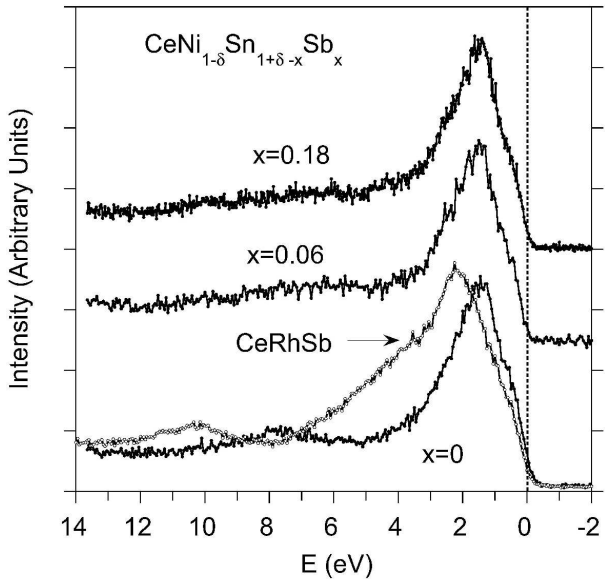

Figure 1
209x297mm (600 x 600 DPI)

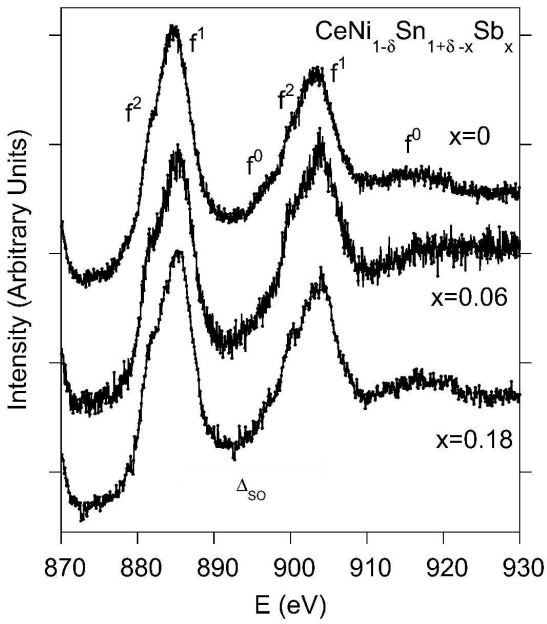

Figure 2
209x297mm (600 x 600 DPI)

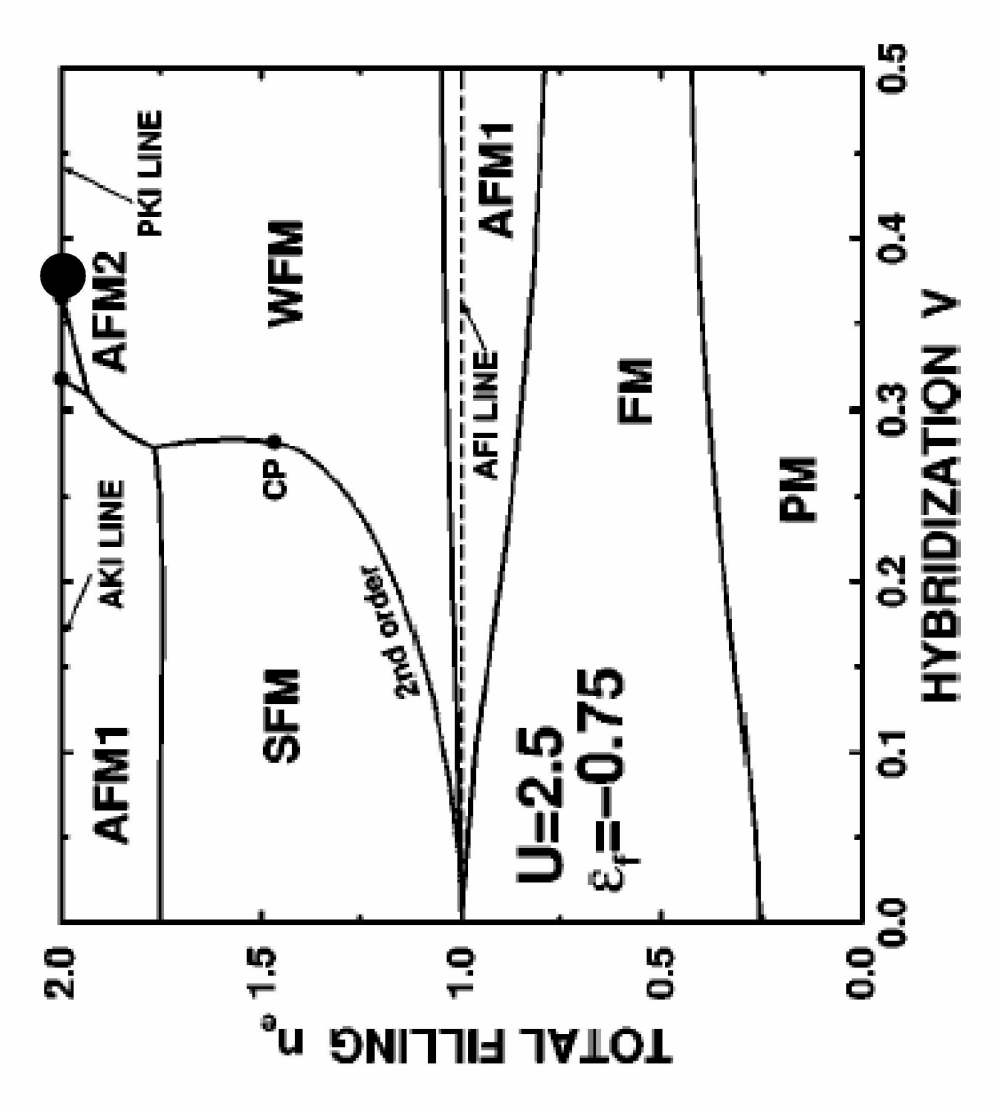

Figure 3
99x110mm (600 x 600 DPI)

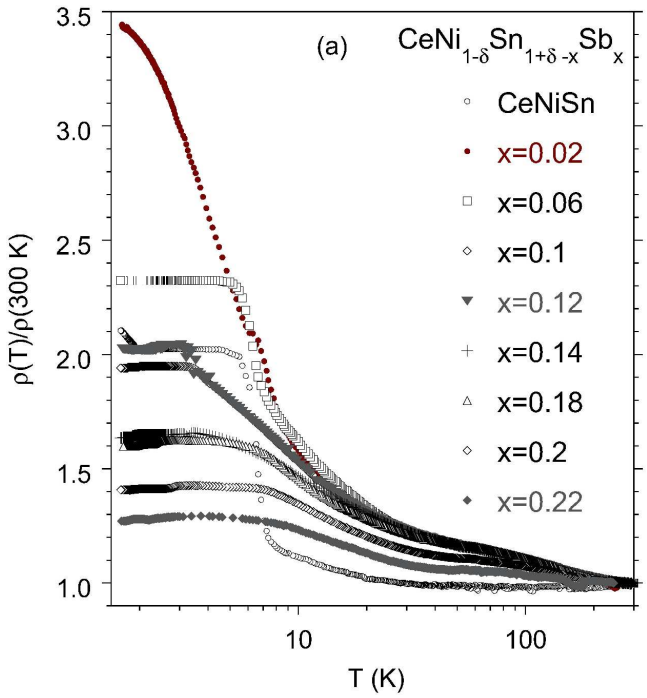

figure 4a
209x297mm (600 x 600 DPI)

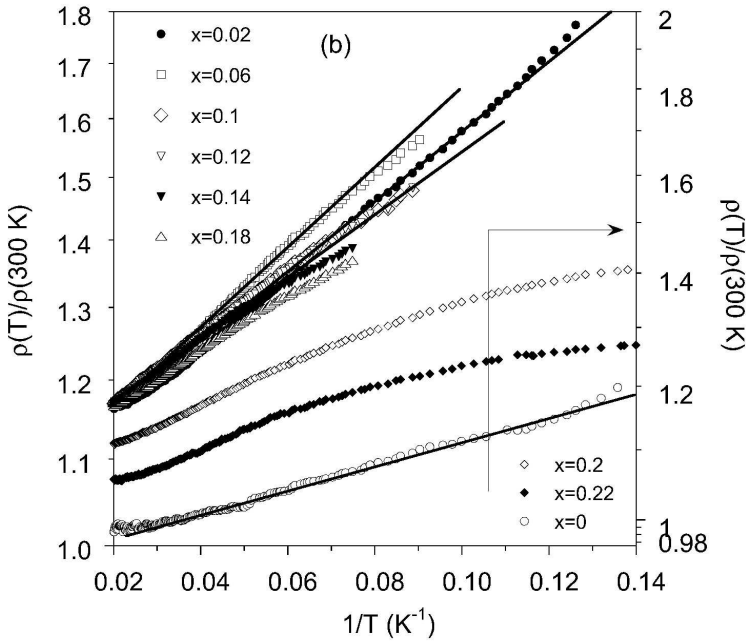

Figure 4b
209x297mm (600 x 600 DPI)

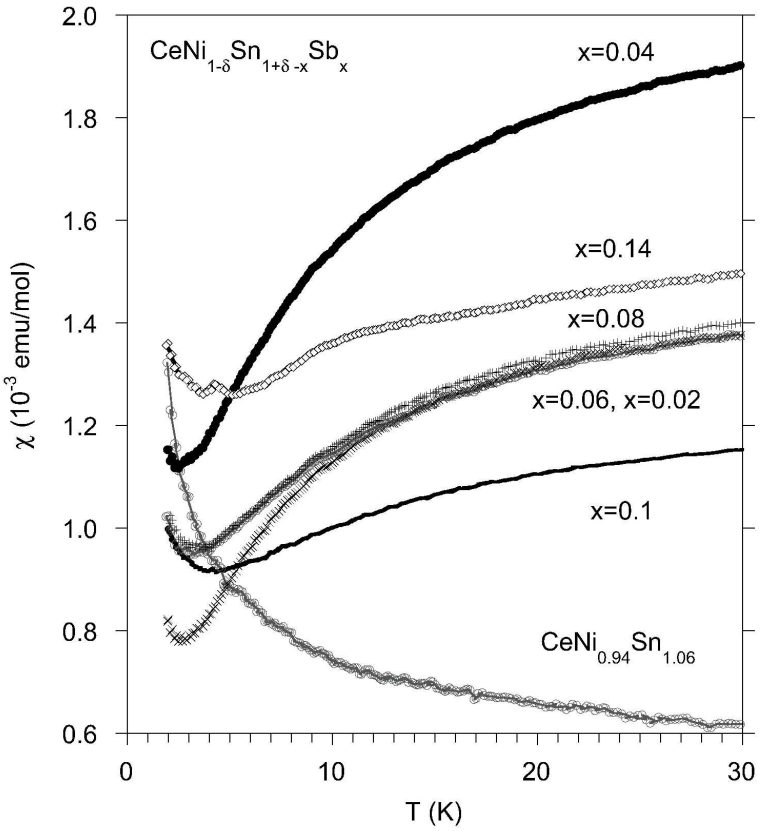

Figure 5
209x297mm (600 x 600 DPI)

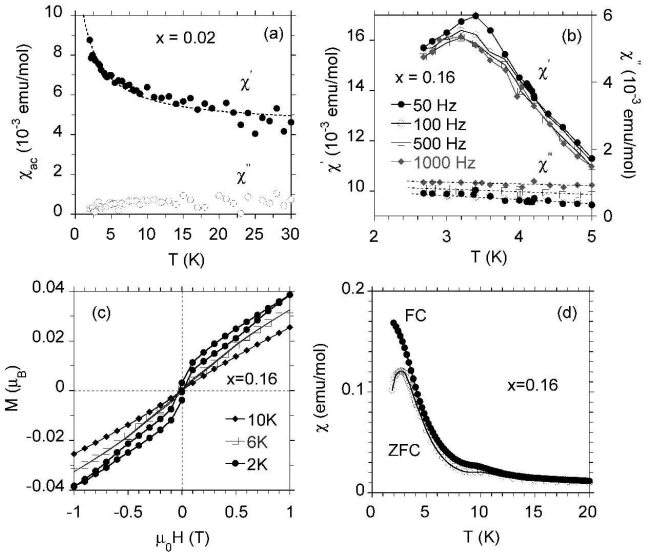

Figure 6
209x297mm (600 x 600 DPI)

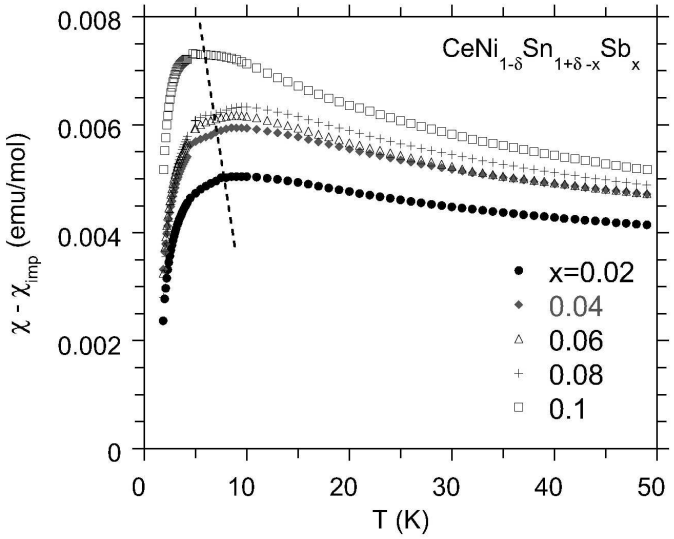

Figure 7
209x297mm (600 x 600 DPI)

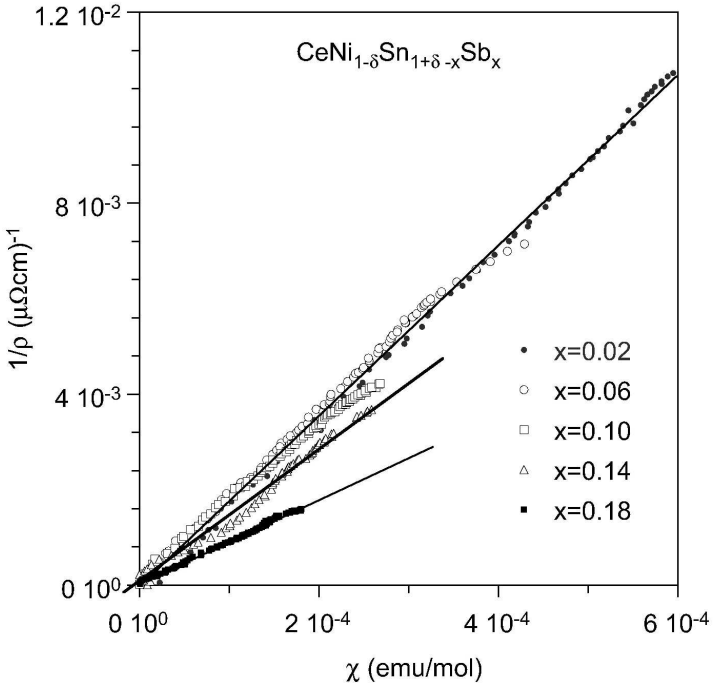

Figure 8
209x297mm (600 x 600 DPI)

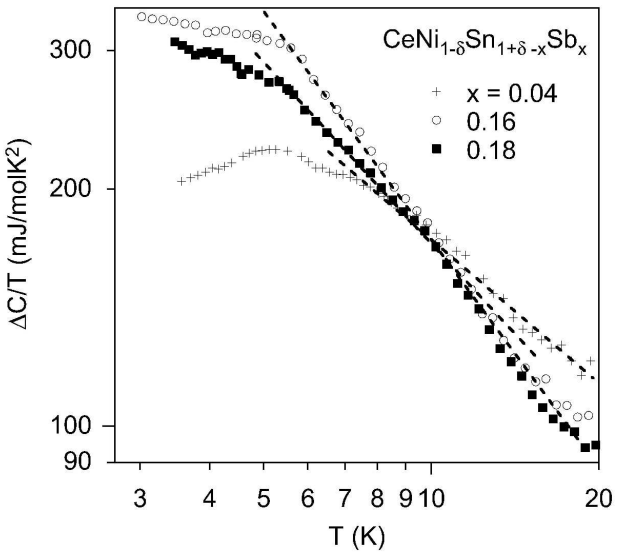

Figure 9
209x297mm (600 x 600 DPI)

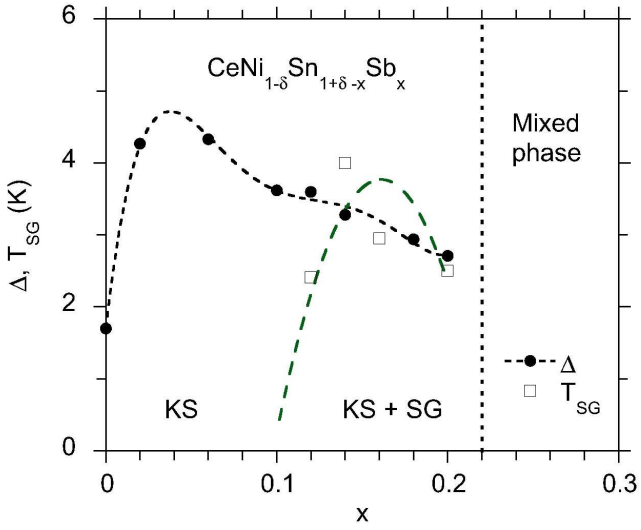

Figure 10
209x297mm (600 x 600 DPI)